Latin American Journal of Solids and Structures
www.lajss.org

Experimental and Numerical Study on the Dispersion Patterns and Penetration Properties of MEFP with Seven Arc-Cone Liners

Abstract

A new MEFP warhead with seven arc-cone liners which can form 7,13 or 19 penetrators at different standoffs is designed. Dispersion patterns and penetration properties of MEFP are performed on five #45 steel targets of dimension 160cm x 160cm x 1.5cm at various standoffs (45cm, 60cm, 80cm, 120cm, 170cm). It reaches the conclusion that every surrounding liner is broken into three penetrators during the formation process of MEFP and a group of aimable penetrators consisting a central projectile surrounded by 18 penetrators is finally formed. Maximum divergence angle of surrounding penetrator is 9.8° and the damage area reaches 0.37m^2 at 1.7m. A nonlinear surface fitting about perforations information on the targets at different standoffs provides a method of predicting the dispersion patterns of MEFP. Once initiated, damage probability for defeating light armor of MEFP warhead with seven arc-cone liners is significantly improved and the results provide important reference to the design and optimization of MEFP warhead in engineering.

Keywords

Multiple Explosively Formed Penetrators (MEFP); Arc-cone liner; Fracture; Dispersion pattern; Penetration

JianFeng Liu [a]
Yuan Long [a]
Chong Ji [a]
Mingshou Zhong [a]
Ying Liu [a]
Xinghua Li [a]

[a] College of Field Engineering, PLA Univ. of Sci.&Tech., China
ljflccc@163.com

* Corresponding Author Email: blastingcaptain@163.com; zhongms7@126.com

http://dx.doi.org/10.1590/1679-78253770

Received 24.02.2017
In revised form 16.04.2017
Accepted 16.04.2017
Available online 20.04.2017

1 INTRODUCTION

Explosively formed penetrator (EFP) is a kind of shaped charge structure which has higher penetration ability and larger standoff. The design and theoretical analysis of EFP is a hot problem in the field of weapon engineering [Cardoso et al.,2016; Johnson et al.,2006; Weickert et al.,1993]. The primary applications are for mining and for the defeat of armor. With the advent of the multiple explosively formed penetrator (MEFP) warhead concept, designers are investigated for a variety of weapon systems [David et al.,2001; William et al.,2002]. Warheads are analyzed and

tested for use in mine clearing, various demolition devices for defeat of diesel fuel drums and light armors[Richard et al.,2005;2010].

MEFP Warhead technology is initiated in the1980's [Richard et al.,2001] to provide a warhead that can produce many highly effective penetrators for the attack of light materiel targets. Previously, EFP warheads are designed to produce a single rod shaped or ball shaped penetrator for deep armor penetration [Yu et al.,1999]. With the MEFP warhead concepts, the charge structure is designed and formed to produce many individual penetrators to attack light materiel targets. A very promising option in the category of anti-missile warhead is a MEFP warhead which can produce focused culster of many penetrators. The high velocity penetrators formed from MEFP warhead can effectively defeat the targets like low flying aircrafts and attack missiles due to increased probablity of hit and greater penetration capability[Weickert et al.,1990].The main design criteria for MEFP warhead is to produce penetrators with high kinetic energy(KE),appropriate shape and high velocity to achieve maximum damage to the target. The axis-symmetric shape of penetrators is not necessary in this case as the warhead is detonated comparatively at small standoff[Blachel et al.,1999]. Initial MEFP warhead concepts utilize a steel case, LX-14 explosive and a tantalum, iron or copper liner to produce the individual penetrators. Penetrator including strips, spheroids, ellipsoids and rods shapes have been designed and tested for various applications. Penetrators weighting from 5 to 50 grams have been provided in various warheads with velocities of 1500 to 2500 m/s[Richard et al.,2001]. And MEFP spray patterns of various sizes and shapes have also been changed to provide focused or directional patterns.

As a key component of MEFP warhead, the liner undergoes extreme yet controlled plastic deformation induced by an explosive. Therefore, the structure and material of liner play an important role in the characteristic parameters of MEFP. A MEFP liner is basically referred to a conventional EFP liner that produces a shotgun like spray of compact fragments. During the formation process, the liner experiences essentially plastic strain up to 300%, at strain rates of the order of 10^4 s^{-1}[Meyers et al.,1994].Tantalum, copper, iron, molybdenum and tantalum–tungsten alloys have been widely used in warhead applications[Pappu et al.,2002]. As for the liner structure, the hemispherical liner and arc-cone liner are the two most commonly used liners in EFP warhead. Using LS-DYNA software, Li et al.[2010] studies the problem of an annular multi-point initiation circuit applied to an EFP warhad with hemispherical liner, and the effects on the penetrator formation parameters by changing the initiation modes. In an EFP impact experiment presented by Wu et al.[2007], a kind of arc-cone liner EFP warhead which can form a high-flying velocity and ideal dimensionless ratio of length and diameter penetrator is optimized and designed. According to the current research results, the hemispherical liner has been widely used in MEFP warhead. A MEFP warhead[Zhao et al.,2013] with seven hemispherical liners is designed to improve the hit probability. Such a warhead can form seven EFPs which have a definite impact direction and can penetrate a 15 mm thick #45 steel(the carbon content is about 0.45%)[Li et al.,1995] target, increasing the number of damage elements and the damage area. Saroha et al.[2010] design a MEFP warhead with seven hemispherical iron liners. In their experiment, the velocities and shapes of penetrators are recorded by using flash X-radiography and mild steel plates are used to evaluate penetration capabilities and dispersion patterns of MEFP. Nevertheless, the literature review clearly reveals that the spatial dispersion patterns and penetration properties at different standoffs of MEFP is limited and incon-

sistent. In particular, reports regarding the investigation on the design and testing of MEFP warheads with arc-cone liners are very few. Therefore, studying the spatial dispersion patterns and penetration properties of the whole process of MEFP formation is crucial.

In the current study, a kind of MEFP warhead consisting of seven arc-cone liners is designed. Compared to conventional MEFP, every surrounding liner of this new MEFP warhead is broken into three penetrators during the formation process and a group of aimable penetrators consisting a central projectile surrounded by 18 penetrators is finally formed. Therefore, the damage probability for defeating light armor can be significantly improved. Dispersion patterns and penetration properties of MEFP are performed on five #45 steel targets of dimension 160cm x 160cm x 1.5cm at various standoffs (45cm, 60cm, 80cm, 120cm, 170cm). Corresponding three-dimensional numerical simulations have been performed to supply and verify the the performance of MEFP.

2 DESIGN AND PARAMETERS OF MEFP WARHEAD

2.1 The Influence Factors of MEFP Formation

(1) *Liner*: The liner is the most important component for the design of MEFP. The structures and properties of the liner are key factors influencing the performance parameters of MEFP. As for the geometric shape of liner, both hemispherical liner and arc-cone liner should be smoothed. Otherwise, the projectile will be distorted during the dynamic formation process of MEFP[Zhao et al.,2013]. The velocity of projectile has a slight increase as the radius of liner curvature grows. The dimensionless ratio of length and diameter of the projectile reduces when the liner thickness increases[Zhao et al.,2016]. The eventual effectiveness of the liner as a projectile is attributed to its high density, high ductility, high strength and sufficiently high melting temperature which prevent melting caused by adiabatic heating[Zhao et al.,2015].

(2) *Explosive loading:* There are two main methods used to load explosive broadly, which are melt-cast and pressed load methods. There should be no space between the explosive and the liner. The charge height is the distance between the top of liner and the detonating fuse, which must be sufficient to ensure detonation wave becomes plane wave when the explosive wave arrives at the liner approximately. Generally, the velocity of MEFP, energy and the penetration depth increase with the increase of the charge height. But the increase of the penetration depth becomes not evident when the charge height increases to a certain extent. The penetration depth does not increase after the height over one and a half times of the charge diameter[Zhao et al.,2013].

(3) *Ignition method:* The ignition method influences formation property of MEFP essentially. Different ignition methods will produce different MEFP even if the other situations are the same, such as the charge and the liner structure. The multi-point ignition method can not only enhance the velocity of the penetrators but also increase the dimensionless ratio of the length and diameter. The liner will be damaged and penetrators will be broken during the formation process because of the interaction between the liners and explosive waves. The radius of multi-point ignition can influence the performance parameters of penetrator, too. Generally, the velocity of penetrators and the dimensionless ratio between length and diameter increase when the ignition radius increases[Zhao et al.,2012].

2.2 Design of MEFP Warhead

An integral-type MEFP warhead with seven arc-cone liner, a booster, and an explosive (Figure 1) is fabricated. The seven sub-liners are located equally in the charge: one is located at the center and the rest are placed around it. The booster is initiated at the center of the back of the central liner, and one-point initiation method is adopted. Figure 2 shows a photograph of the MEFP charge.

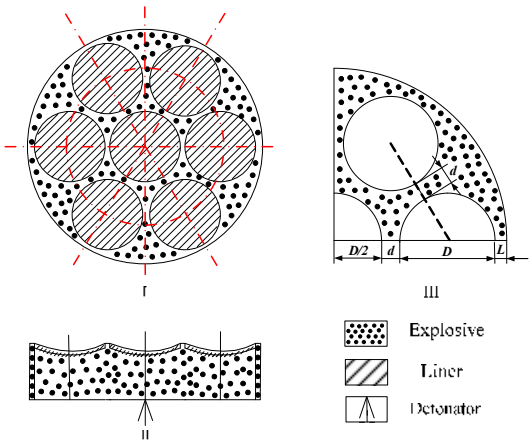


Figure 1: Configuration of MEFP charge.

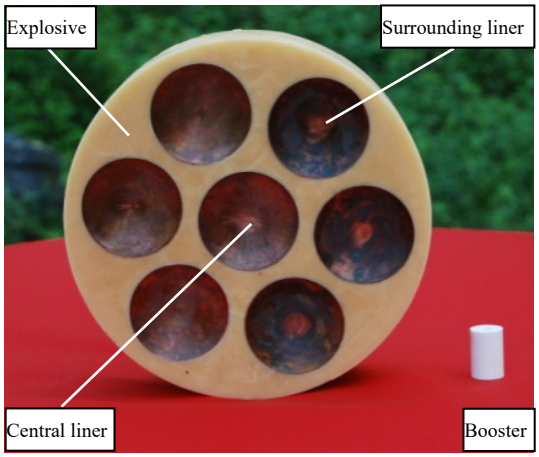


Figure 2: Photograph of MEFP charge.

The explosive is a cylinder of radius R_0 with seven round holes, which are used to install sub-liners and match the size of these sub-liners well. As shown in Section III of Figure 1, the explosive radius R_0 is expressed by

$$R_0 = L + D + d + \frac{D}{2} \tag{1}$$

In Eq. (1), L is the minimum distance from cylindrical hole surface to explosive cylinder surrounding surface; D is the diameter of round holes equal to the caliber of the liner; and d is the minimum distance between each cylindrical hole surface, namely, the space between neighboring sub-liners.

The materials of MEFP charge and basic parameters dimension of liner are shown as follows:

(1) *Explosive*: The high explosive is Comp B with a nominal density of 1.717 g/cm^3 and a detonation velocity of 7980 m/s. The total weight of the explosive is 3724g. [Zhao et al., 2013].

(2) *Liner*: An arc-cone liner is imparted into produce the individual penetrator. The diameter of the charge liner is 56 mm. Both outer and inner curvature radius of liner (as shown in Figure 3) is 46mm. Considering the cost efficiency, we choose oxygen-free high-conductivity copper (OFHC) liner with tensile strength of 35-45% and ductility of 45%[Zhao et al., 2015]. The liner weighs 69.4 g.

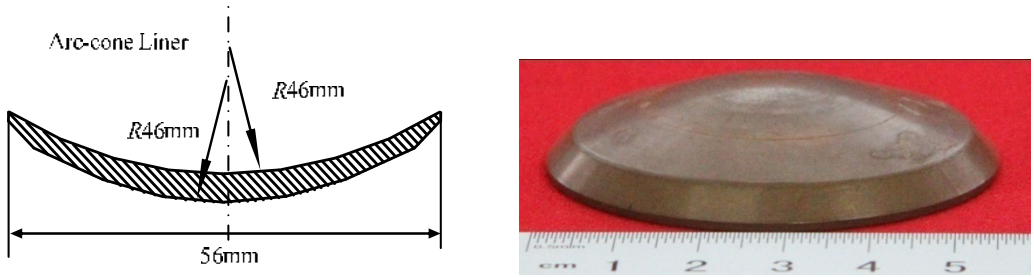


Figure 3: Structure of the liner.

2.3 Definition of MEFP Divergence Angle and Damage Area

To facilitate analysis, the maximum divergence angle a and damage area S_z are used to measure and describe the radial dispersion of MEFP at different standoffs. A spatial rectangular coordinate system ($\vec{x}$-$\vec{y}$-$\vec{z}$) is established along the charge. A coordinate origin (0, 0, 0) is selected at the top central of the charge. Figure 4 displays a sketch map of the divergence angle a and damage area S_z.

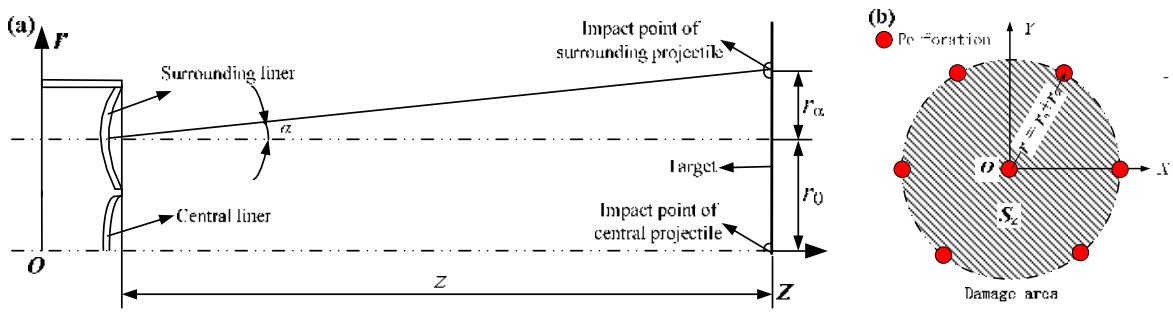


Figure 4: Sketch map of the divergence angle and the damage area.

Divergence angle a indicates that the radial dispersion of MEFP can be expressed by

$$\alpha = arctg\frac{r}{z} \tag{2}$$

In Eq. (2), standoff z is the distance from the central of the MEFP warhead to the target plate; and r is the radial dispersion of penetrators, which could be determined by Eq. (3)

$$r = r_0 + V_r\, t \tag{3}$$

In the equation, r_0 is the distance between the central liner and the surrounding liner, r_0 = 0.07m; V_r is the radial velocity of surrounding penetrator; t is the time before the penetrator hits the target and can be determined by the following equation

$$t = \frac{z}{V_x} \tag{4}$$

In the equation, V_x is the axial velocity of surrounding penetrator, so the divergence angle a is determined by Eqs. (2)-(4).

As shown in Fig. 4(b), the sketch map of the damage area is expressed by S_z

$$S_z = \pi r^2 \tag{5}$$

Damage area S_z is determined by Eqs. (3)-(5) and it can be viewed as the area covered by the surrounding penetrators at different standoffs.

3 EXPERIMENTAL INVESTIGATIONS

3.1 Experimental Setup and Program

We carried out experiments of MEFP warhead against #45 steel target in order to verify dispersion patterns and penetration properties of MEFP. Two #45 steel targets of 1.5cm thickness were positioned in front of MEFP warhead at different standoffs. The distance between the two target is 1m. Figure 5 illustrates the schematic sketch of the experiment.

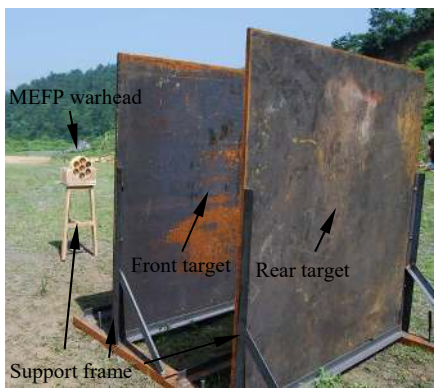


Figure 5: Experimental setup of MEFP warhead against #45 steel target.

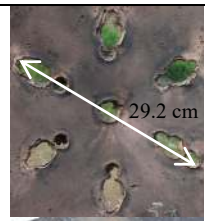
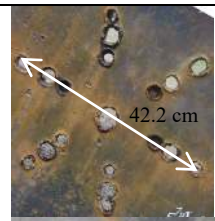
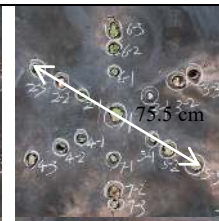
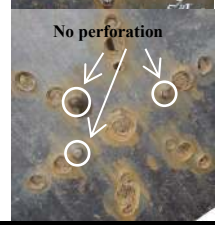
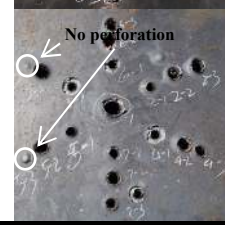
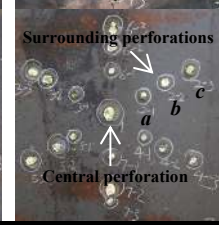
The MEFP warhead will be placed on a special wooden support frame after the front target and rear target are set up. The central of MEFP warhead and front target are in the same horizontal plane by adjusting aiming sight and level gauges. Five kinds of projects designated 1, 2, 3, 4, 5 are designed according to varies standoffs. Five experiment projects are given in Table 1. Experiments are carried out in order to verify penetration ability of MEFP and dispersion state of surrounding penetrators.

Project	1	2	3	4	5
Standoff z/ m	0.45	0.6	0.8	1.2	1.7

Table 1: Experimental projects.

3.2 Results and Discussion

Perforations on witness target at different standoffs are present in Table 2. There are three interaction modes of MEFP against targets at different standoffs according to experimental results which mean three fractures occur during the formation process of MEFP.

z /m	0.45	0.60	0.80	1.20	1.70
Front view					
Rear view					

(Due to the geometric structure design, material selection and machining techniques of the liner and explosive, surrounding perforations in the steel target are not completely symmetrical in the experiment. Here we treat surrounding perforations as the same shape.)

Table 2: Perforations on the witness targets at different standoffs.

(1) Seven perforations are recorded on the target when standoff is 0.45m. It indicates that seven penetrators have been formed at this movement. #45 steel target subjected to normal impact by central EFP and oblique impact by surrounding penetrator.

(2) Two perforations along the radial distribution appeared for a surrounding penetrator at 0.6m. There is a radial velocity difference in surrounding penetrator, which directly leads to the fracture of the penetrator.

(3) As the standoff reaches 0.8m, 19 perforations appear on the #45 steel target. Every surrounding penetrator will be broken into three sub-penetrators. Fragments group contains 19 fragments which consists of three sub-fragments groups surrounding the center penetrator in the radial distribution. These sub-fragments cause three groups of surrounding perforations on the target (Surrounding perforations a, Surrounding perforations b and Surrounding perforations c, presented in Table 2 at 1.7m).

Based on dispersion information of perforations on the target, we can get divergence angle and damage area of MEFP by equation (2) and equation (5), as shown in Figure 6 and Figure 7. There are two perforations along the radial distribution for surrounding penetrators at 0.6m. Figure 6 displays divergence angle of MEFP. Divergence angle appears during the flight distance of MEFP. Minimum divergence angle of fragments group a is 3.4°, divergence angle of fragments group b is about 7° and maximum divergence angle of fragments group c is 9.8°. Damage area of MEFP is

presented in Figure 7 and increases rapidly with increasing of standoff. The maximum damage area is 0.37m^2 when the standoff reaches 1.7m.

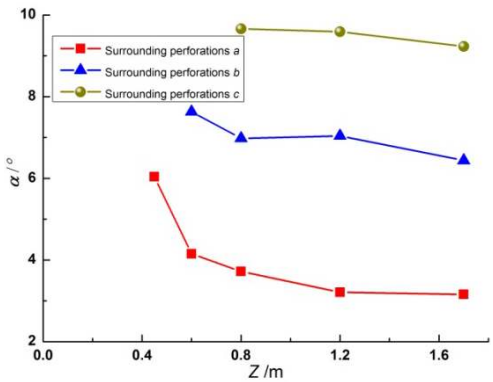


Figure 6: Divergence angle of MEFP (Experimental results).

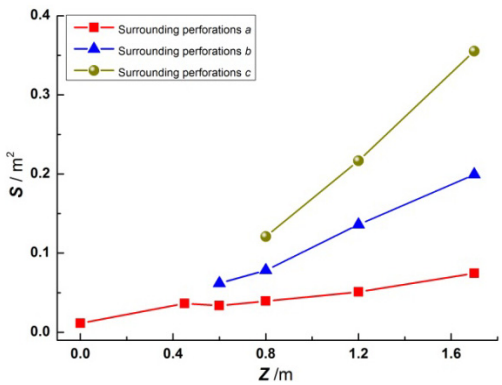


Figure 7: Damage area of MEFP (Experimental results).

As the standoff increases, damage probability can be significantly improved due to the increase of fragments in per unit area and this MEFP warhead has an intensive attack on thin armor. Spatial distribution of MEFP perforations on the target are given in Figure 8. The shape of all perforations on the targets at different standoffs is just like a inverted cone.

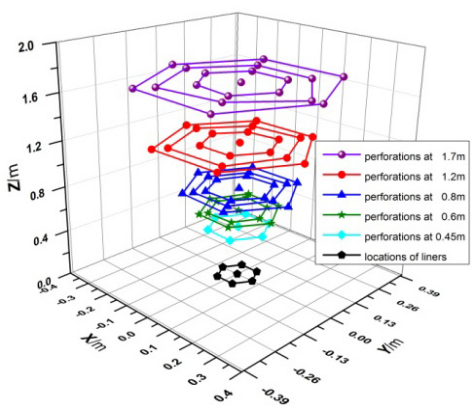
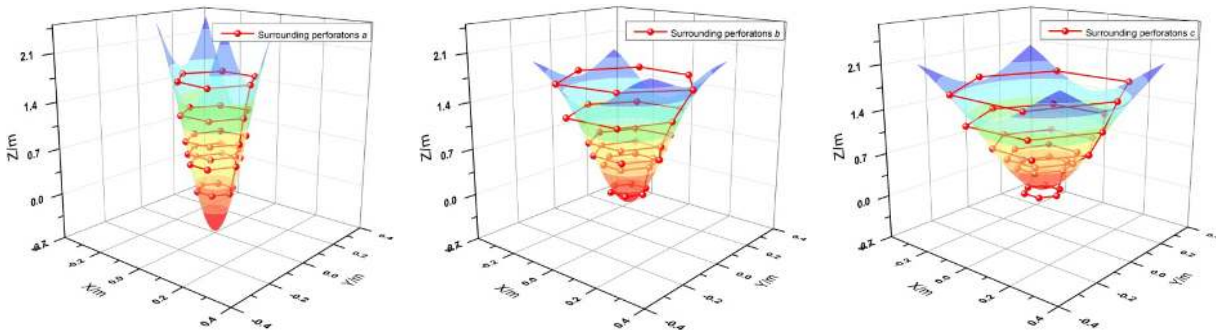


Figure 8: Spatial distribution of MEFP perforations on the targets.

Based on the perforations information on the front targets at different standoffs, surface fitting function of Gauss model is adopted to carry on three-dimensional surface fitting. And then the characterization of the fitting surface is obtained, as shown in Figure 9.



(*a*) Surrounding perforations *a* (*b*) Surrounding perforations *b* (*c*) Surrounding perforations *c*

Figure 9: Nonlinear surface fitting of perforations on the targets.

Model of spatially perforations is obtained, as shown in equation (6),

$$Z = Z_0 + Ae^{-\frac{1}{2}(\frac{X-C_1}{W_1})^2-\frac{1}{2}(\frac{Y-C_2}{W_2})^2}, (Z \geq 0) \tag{6}$$

For the surrounding perforations *a*, Z_0=3.28, A=-3.95, C_1=0.00088, C_2=0.00080, W_1=0.11, W_2=0.12. For the surrounding perforations *b*, Z_0=2.09, A=-2.27, C_1=0.0020, C_2=-0.0021, W_1=0.14, W_2=0.15.

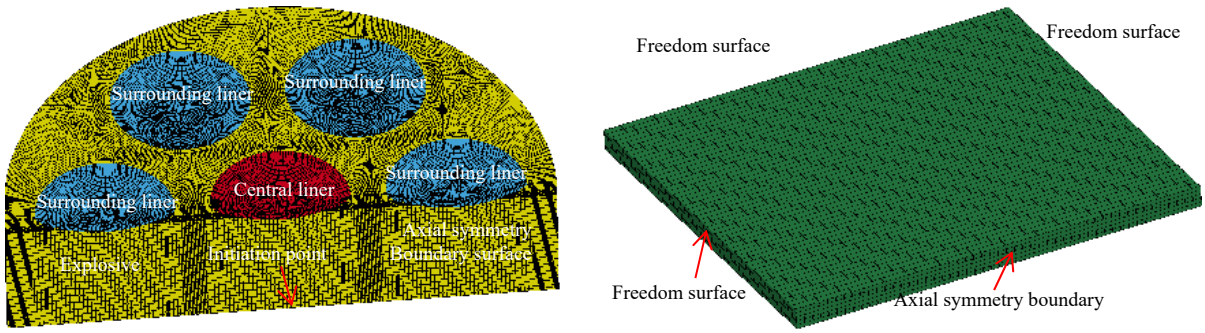
For the surrounding perforations *c*, Z_0=2.40, A=-2.33, C_1=0.0048, C_2=-0.0037, W_1=0.22, W_2=0.22. Unit is *m*. Coefficient of determination(R^2) is 0.96, 0.95, 0.95, respectively.

Laws of spatially perforations are obtained by a nonlinear fitting method. It provides an effectively method to predict spatial distribution and forecast damage area of MEFP. The central liner can form an EFP has a good aerodynamic shape at different standoffs. Surrounding liner can form a distorted EFP at early time of MEFP formation. Each surrounding liner will be broken when the standoff is about three times charge caliber. MEFP warhead can form a fragments group contains 19 perforations which has the ability to breakdown a 1.5cm thickness steel target at 1.7m. As the standoff increases, dispersion pattern model of MEFP is obtained, just as described in equation (6). It will be easily to forecast damage area if the distance between the target and the warhead can be measured. Furthermore, damage probability can also be determined then.

4 NUMERICAL SIMULATION MODEL AND PARAMETERS OF MATERIALS

4.1 Establishment of the Simulation Model

Numerical simulation is carried out using three-dimensional (3D) dynamic finite element program of LS-DYNA in order to study the formation and dispersion patterns of MEFP. The simulation models of the MEFP warhead and the target are presented in Figure 10. Due to symmetry, modeling 1/2 of the geometry is necessary to simplify the analysis and reduce the computational cost.



(a) MEFP warhead (b) Target

Figure 10: Simulation model of MEFP warhead and target(1/2 model).

The explosive, liner, and steel target are meshed by Lagrangian algorithm with hourglass control. In order to improve the quality of the discrete elements, numerical models are discretized with 8-node hexahedral solid elements(SOLID164). [Hallquist,1997; Cardoso et al.,2016] For a circular liner in an axisymmetric MEFP warhead, Figure 10 shows the gridding results considered in our study. This approach provides elements that are approximately equally sized, but some asymmetries are introduced and some elements are not formed in a compact manner. In an effort to introduce more symmetry into the grid, it is possible to put uniform rings around the outer portions of the circle, as shown in the meshing process of liners. This provides the same number of elements in each of the uniform rings. Here the asymmetries are reduced, but the elements get larger and larger as they move outward (for a constant radial increment), as shown in Figure 10 (a). [Hallquist,1997; Johnson et al.,2006] *BOUNDARY_SPC_SET [Hallquist,1997] is used in the simulation model to restrict elements movement in the symmetrical boundaries. The symmetrical inhibit condition is added to the symmetrical surface of the model to restrict the node's displacement and rotation degrees of freedom. Contact may occur along the surfaces of a single body undergoing large deformation, between two or more deformable bodies, or between a deformable body and a rigid barrier. *CONTACT_SLIDING_ONLY_PENALTY [Hallquist,1997] is used to model the impact between the dynamite and liners. The contact keyword between the penetrators and the target is changed to *CONTACT_ERODING_ SURFACE_TO_SURFACE. A large number of numerical calculation results can prove that detonation products at about 30 μs will no longer affect the characteristic parameters of MEFP after the explosive is detonated. Therefore, the explosive is deleted at 30 μs in the numerical calculation [Li et al., 2010].

4.2 Material Constitutive Models and Parameters

4.2.1 Material Model for High Explosive

High explosives (Comp B) are typically modeled by using the Jones-Wilkins-Lee (*JWL*) EOS, which models the pressure generated by chemical energy in an explosion. It can be written in the form

$$p = A_1\left(1-\frac{\omega}{R_1 v}\right)e^{-R_1 v} + B_1\left(1-\frac{\omega}{R_2 v}\right)e^{-R_2 v} + \frac{\omega e}{v} \tag{7}$$

where p is the hydrostatic pressure; v is the specific volume, e is internal specific energy. The values of constants A_1, R_1, B_2, R_2, ω for many common explosives have been determined from dynamic experiments.

4.2.2 Material Model for Copper and #45 Steel

To be able to describe the various phenomena taking place during contact explosion, it is necessary to characterize the behavior of materials under explosion-generated high strain rate loading conditions. Liners and target are both modeled by the Johnson-Cook (*J-C*) material model[Johnson and Cook,1983], which is suitable to model the strength behavior of materials subjected to large strains, high strain rates and high temperatures. The model defines the yield stress σ_y as

$$\sigma_y = \left[A + B\left(\bar{\varepsilon}^p\right)^n\right]\left[1 + C\ln\dot{\varepsilon}^*\right]\left[1-\left(T^*\right)^m\right] \tag{8}$$

where A,B,C, n and m are the material parameters determined by experiments. $\bar{\varepsilon}^p$ is the equivalent plastic strain, $\dot{\varepsilon}^* = \dot{\varepsilon}_p / \dot{\varepsilon}_0$ is the dimensionless effective strain rate at a reference strain rate $\dot{\varepsilon}_0 = 1 s^{-1}$. T^* is the homologous temperature which is defined by $T^* = \left(T - T_{\text{room}}\right)/\left(T_{\text{melt}} - T_{\text{room}}\right)$, where T is the current temperature, T_{room} and T_{melt} are the room and melting temperatures, respectively.

Johnson and Cook [Johnson and Cook,1985] also developed a failure criterion that accounts for temperature, strain rate and strain path in addition to the triaxiality of the stress state. The model is based on damage accumulation, and has the basic form

$$D = \sum \frac{\Delta\varepsilon_y}{\varepsilon_f} \tag{9}$$

where D is the damage to a material element, $\Delta\varepsilon_y$ is the increment of accumulated plastic strain, and ε_f is the accumulated plastic strain to failure under the current conditions of stress triaxiality, strain rate and temperature. Failure occurs when D=1, and in the finite element simulations, element erosion is used to remove elements that have reached the critical damage. The failure strain ε_f is defined as

$$\varepsilon_{\text{f}} = [D_1 + D_2 \exp D_3\sigma^*][1 + D_4 \ln\dot{\varepsilon}^*][1 + D_5 T^*] \tag{10}$$

where σ^* is the dimensionless pressure-stress ratio defined as $\sigma^* = \sigma_{\text{m}}/\bar{\sigma}$, where σ_{m} is the mean stress normalized by the effective stress, $\bar{\sigma}$ is the effective stress, and D_1, D_2, D_3, D_4 and D_5 are the material parameters[Johnson and Cook,1985; Chen et al., 2007]. Details of finite element modeling of Comp B, copper liner and target are described in Table 3[Zhao et al., 2016; Li et al., 2010].

Comp B	ϱ (g/cm^3) 1.717	D (km/s) 7.98	P_{CJ} (GPa) 29.5	A_1 (GPa) 524.23	B_1 (GPa) 7.678	R_1 4.20	R_2 1.1	ω 0.34	E_0 (GPa) 0.085	V_0 1.00
	ϱ (g/cm^3) 8.97	G (GPa) 46.50	A(MPa) 90	B(MPa) 292	N 0.31	C 0.025	m 1.09	T_m 1356	σ_s (GPa) 0.09	C (km/s) 3.94
Copper	S_1 1.49	S_2 0	S_3 0	γ_0 2.02	a 0.47	E_0 0	V_0 1.0			
	D_1 0.54	D_2 4.89	D_3 -3.03	D_4 0.014	D_5 1.12					
	ϱ (g/cm^3) 7.83	G (GPa) 77.00	A(MPa) 792	B(MPa) 510	N 0.26	C 0.014	m 1.03	T_m 1793	σ_s (GPa) 0.09	C (km/s) 4.569
#45 steel	S_1 1.49	S_2 0	S_3 0	γ_0 2.17	a 0.46	E_0 0	V_0 1.0			
	D_1 0.1	D_2 0.76	D_3 1.57	D_4 0.005	D_5 -0.84					

Table 3: Parameters of each material.

5 NUMERICAL STUDY ON THE DISPERSION PATTERNS AND PENETRATION PROPERTIES OF MEFP

5.1 Formation Process and Dispersion Pattern of MEFP

For one point initiated MEFP charge, detonation front will first have a normal impact to the central liner and maximum momentum will be given to this liner. The liners positioned in outer side will be distorted because they are subjected to unsymmetrical detonation pressure[Ye et al.,2003; Wang et al.,1998]. In fact, materials will fail if the stress suffered as penetrator stretching exceeds the material yield limit. Surrounding penetrator obtains a radial velocity during oblique impact. All surrounding penetrators are travelling in a radial divergence angle toward the target with same velocity. Table 4 demonstrates the formation process of MEFP at different standoffs.

In the simulation, the first obvious breakage phenomena of all surrounding penetrators appear when the standoff is up to 0.6m and the second breakage phenomena shows as the standoff reaches 0.8m. Three penetrators groups (Surrounding penetrators *a*, Surrounding penetrators *b* and Surrounding penetrators *c*, as shown in Table 4 at 1.7m) surrounding a large dimensionless ratio of EFP in the radial distribution have been formed at last. Surrounding penetrators dispersed at r_a, r_b and r_c, respectively. Observing the formation process of MEFP, including the extension results and break-up of the surrounding penetrators, the results of simulation are in good agreement with the experimental results.

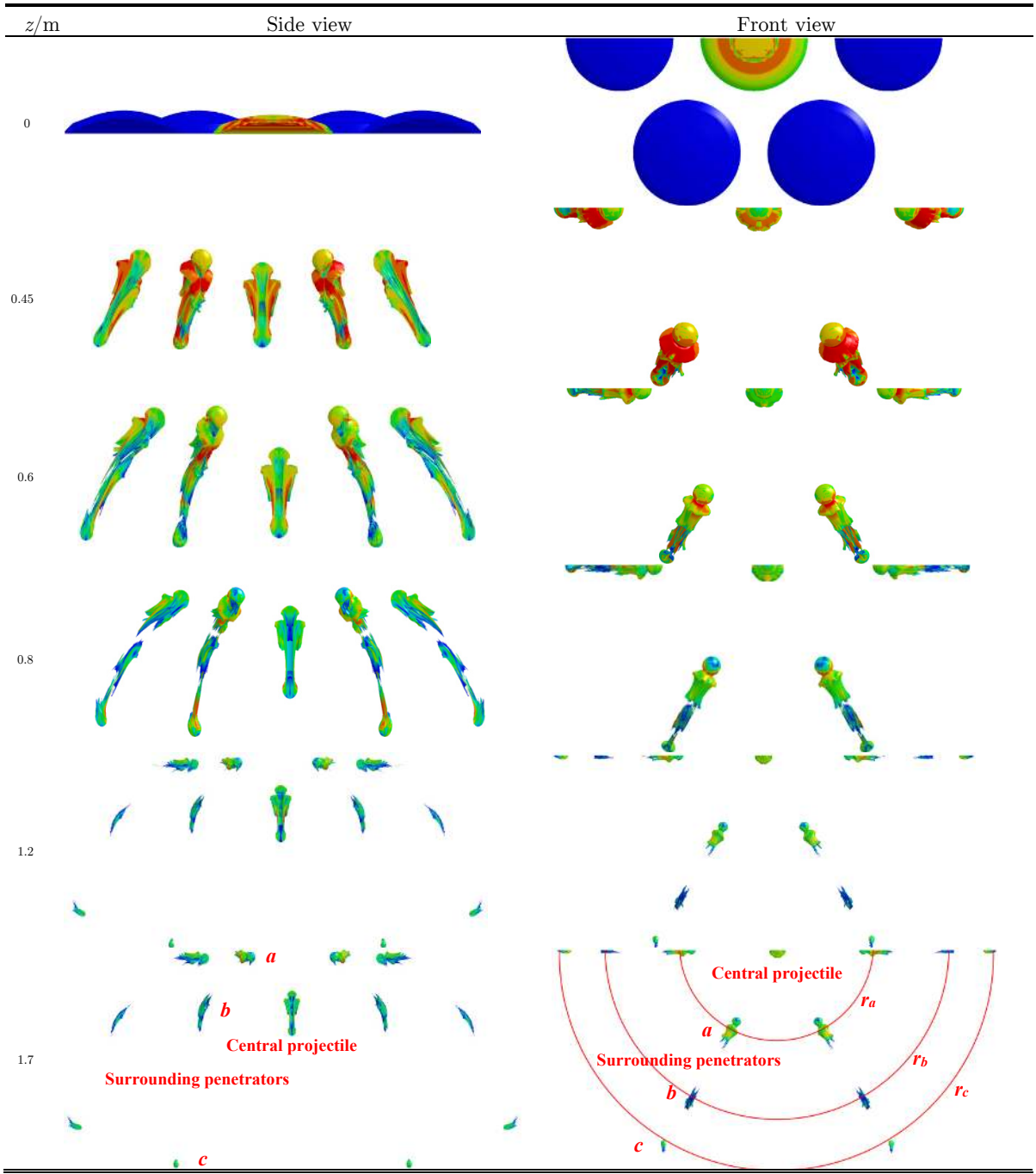


Table 4: Formation process of MEFP at different standoffs (1/2 model).

Figure 11 gives mass change curves of central and surrounding penetrator. m_c is the mass of central penetrator, m_s is the mass of surrounding penetrator. The central liner has a slight loss of quality during the formation process of MEFP because detonation wave has a normal impact to the surface of central liner. It accounts for about 8% of the total mass of the liner. Maximum loss of mass happens on surrounding liner due to the interaction between unsymmetrical detonation wave

and the liner and the mass loss is about 25.3% of the liner. And three penetrators have been formed when the total mass does not change. Figure 12 displays radial and axial velocity of MEFP. V_z is the axial velocity of surrounding penetrator and V_r is the radial velocity of surrounding penetrator.

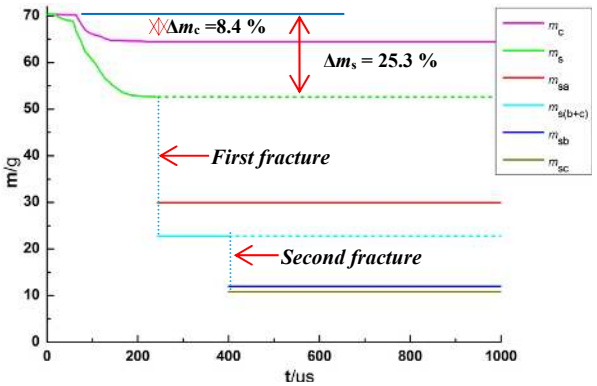


Figure 11: Mass changes of central and surrounding penetrators.

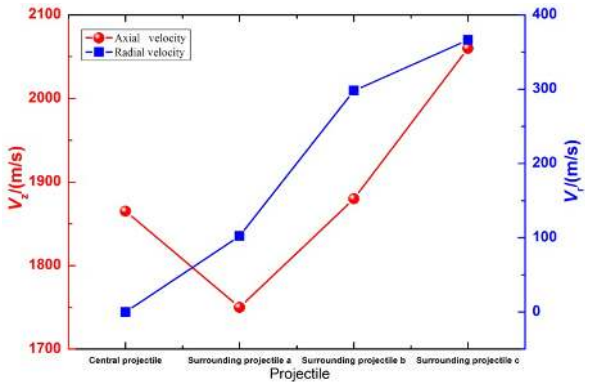


Figure 12: Radial and axial velocity of penetrators.

Divergence angle and damage area of MEFP during the formation process are presented in Figure 13 and Figure 14. The average radial divergence angle is numerically predicted to be 3.38°, 6.4°, 9.93° and the damage area experiences 0.032m^2, 0.13m^2, 0.28m^2 at 1.7m for surrounding penetrators a, surrounding penetrators b and surrounding penetrators c, respectively. Damage area of MEFP increases rapidly as the standoff grows and it is about linear distribution of three surrounding penetrators along radial.

Simulation results of spatial distribution pattern of MEFP have shown excellent agreement with perforations on the front target. It also shows the reasonable of selected numerical models and accuracy of material parameters.

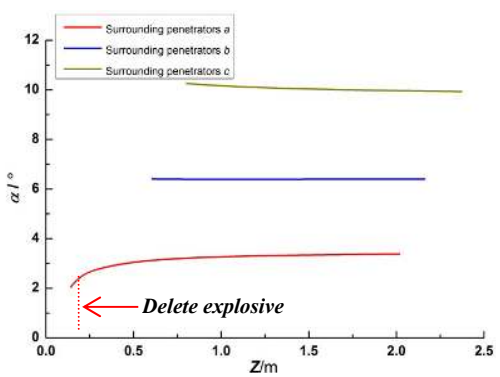


Figure 13: Divergence angle of MEFP (Simulation results).

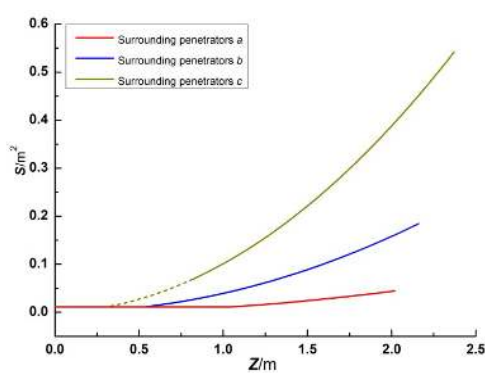


Figure 14: Damage area of MEFP (Simulation results).

5.2 Penetration Process and Dispersion Pattern of MEFP

Further research on the penetration properties and dispersion patterns of MEFP has been carried out at different standoffs. Simulation results of MEFP against #45 steel targets are given in Table 5. Both central penetrator and surrounding penetrators can effective break down a 1.5cm thick #45 steel target at different standoffs in the five numerical schemes according to the experiment settings and it shows the same distribution pattern with the experimental results.

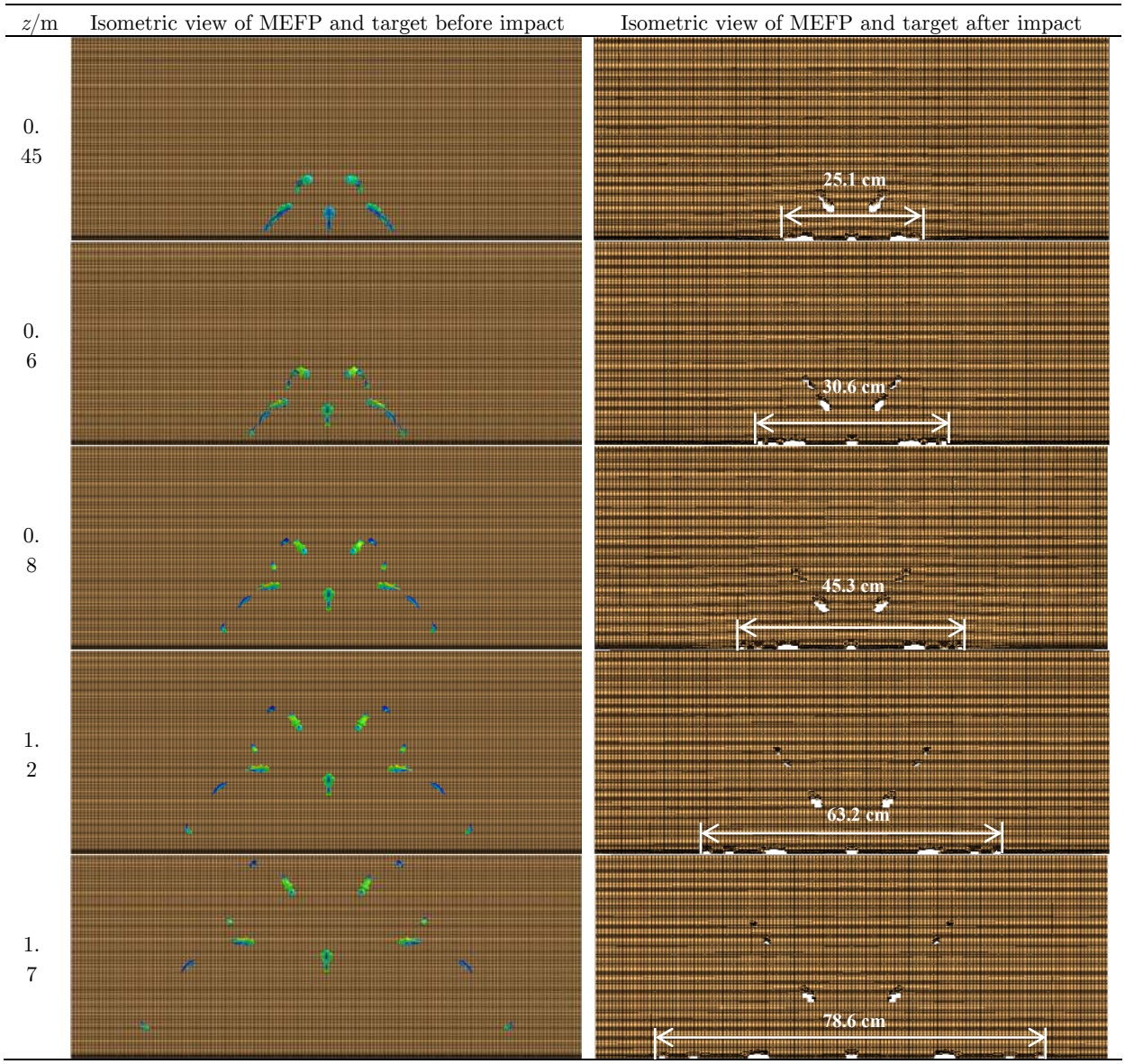
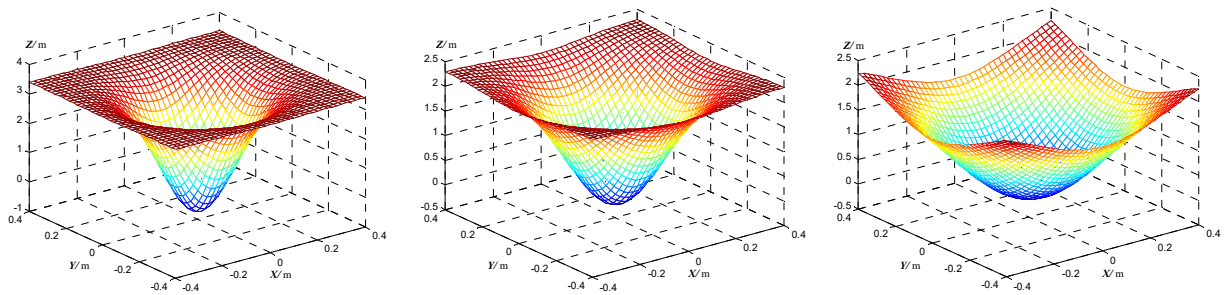


Table 5: Simulation results of MEFP against #45 steel targets at different standoffs (1/2 model).

Dramatic changes occur in surrounding liners of MEFP at 0.6m-0.8m standoffs and each of surrounding liner breaks into three penetrators according to the numerical results. However, it is

meaningless to study the process of formation and penetration properties of MEFP in this interval standoff. But it is particularly important to have a specialize in the dispersion patterns and penetration properties of MEFP before or after the penetrator breaks. Besides, There are a large number of MEFP remainder after a penetrator breaks down the target. So we conduct a study on the penetration properties of MEFP before or after the surrounding penetrator has broken.

Observations on targets and measurements of damage area in simulation(Selected a group of perforations along radial), a nonlinear surface fitting process is also carried out for the perforations based on Gauss model. Figure 15 displays a nonlinear fitting picture of perforations on the targets.



(a) Surrounding penetrators a (b) Surrounding penetrators b (c) Surrounding penetrators c

Figure 15: Track of MEFP spatial movement.

Model of dispersion patterns is obtained, as shown in equation (11),

$$Z = Z_0 + Ae^{-\frac{1}{2}(\frac{X-C_1}{W_1})^2-\frac{1}{2}(\frac{Y-C_2}{W_2})^2} \quad (Z \geq 0) \tag{11}$$

For the surrounding perforations *a*, Z_0=3.40, A=-4.12, XC= YC=0, W_1= W_2=0.13.

For the surrounding perforations *b*, Z_0=2.31, A=-2.52, XC= YC=0, W_1= W_2=0.17.

For the surrounding perforations *c*, Z_0=2.66, A=-2.73, XC= YC=0, W_1= W_2=0.29. Unit is *m*. Coefficient of determination(R^2) is 0.99, 0.99, 0.99.

The surrounding penetrators *a* have a slight increase while the surrounding penetrators *c* have a bigger radial movement. This means that the spatial extent of outer penetrators is bigger and damage area of outer penetrators is larger. The numerical results verify the accuracy law of MEFP spatial distribution.

5.3 Penetration Properties and Dispersion Patterns of MEFP

5.3.1 Model I: No Fracture of Surrounding Penetrator (Z<0.6m)

Results of experiment and simulation of MEFP penetration property at 0.45m are shown in Table 6. There is no fracture of surrounding penetrators in this model and seven perforations left on the target. Oblique penetration by surrounding penetrators has left six oval perforations which can reflect the cross section area of penetrator. A violent interaction between the penetrators and target occurs since copper material appears at the entrance of the target and attaches to the wall of the

target. Fragments of penetrators and debris falling from front target will continue to damage rear target. The central penetrator can effectively break down two layers of #45 steel targets but the surrounding penetrators can not.

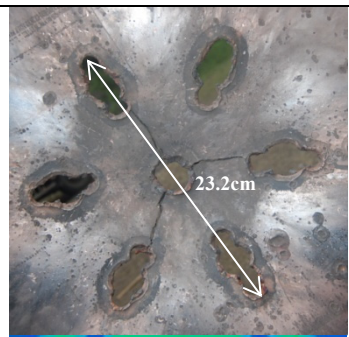
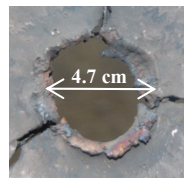
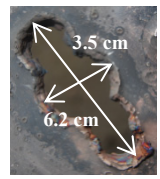
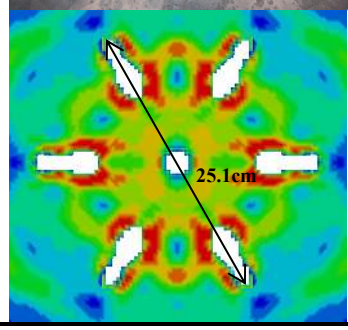
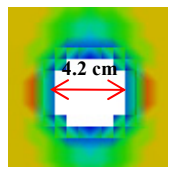
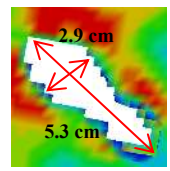
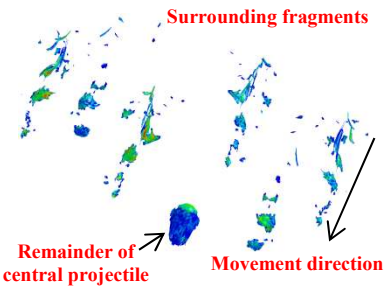
	Perforation pattern recorded on the front target			Rear target and fragments pattern
	Front view	Central perforation	Surrounding perforation	
Experiment				
Simulation				

Table 6: Experimental and numerical results of MEFP penetration properties at 0.45m.

Figure 16 displays the energy changes of central and surrounding penetrator during the formation and penetration process of MEFP. As can be seen from figure 16, energy reduction of central penetrator is much smaller than surrounding penetrator. The contact area between surrounding penetrator and target increases as the target is subjected to normal penetration by central penetrator and oblique penetration by surrounding penetrator. Surrounding penetrator need more energy to break down the same thickness of steel target compared with central penetrator.

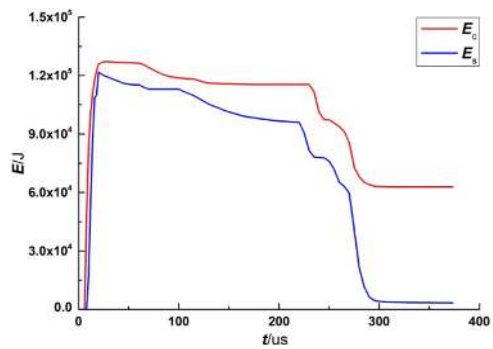


Figure 16: Energy changes of central and surrounding penetrator when the standoff is 0.45m.

5.3.2 Model II: Fracture of surrounding penetrator(Z≥0.6m)

As another typical pattern of MEFP formation, every surrounding penetrator start to break when the standoff reaches 0.6m. Results of experiment and simulation of MEFP penetration property at 1.7m are compared in Table 7. 19 fragments are generated that can effectively break down a #45 steel target with 1.5cm thickness. Every surrounding penetrator will be broken into three sub-penetrators in the radial distribution at 1.7m. The shape of perforation on the target is close to a circle. Three sub-penetrators groups surrounding the center EFP are distributed in the radial direction. Fragments distribute in a more reasonable range against a target. The probability of hitting target has been significantly improved. Damage capacity of surrounding penetrators declines slightly as flip occurs during the flight (penetrators *c*). Compared with the fragments distribution pattern between table 6 and table 7, it is relatively concentrated when the standoff is 0.45m.

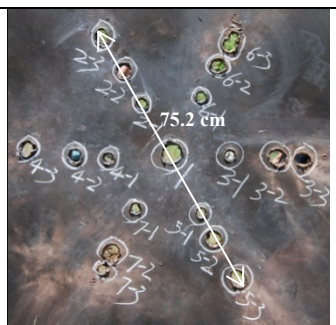
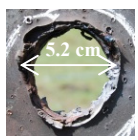
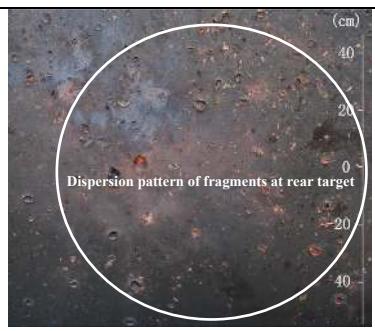
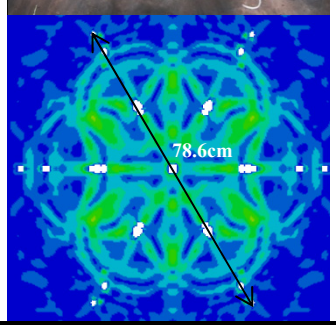
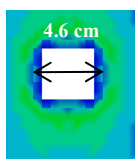
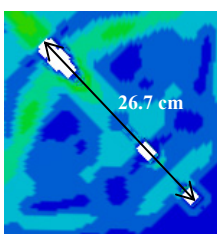
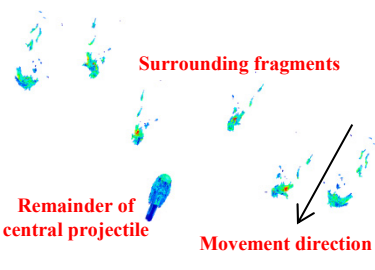
	Perforation pattern recorded on the steel target			
	Front view	Central perforation	Surrounding perforation	Rear target and fragments pattern
Experiment				
Simulation				

Table 7: Experimental and numerical results of MEFP penetration properties at 1.7m.

Energy changes of central and surrounding penetrators during formation and penetration process is presented in Figure 17. As can be seen from the figure, it is only one interaction between central penetrator and target but three times interaction between surrounding penetrator and target when the standoff is 1.7m. Kinetic energy reduction of central penetrator is smaller than that of surrounding penetrator.

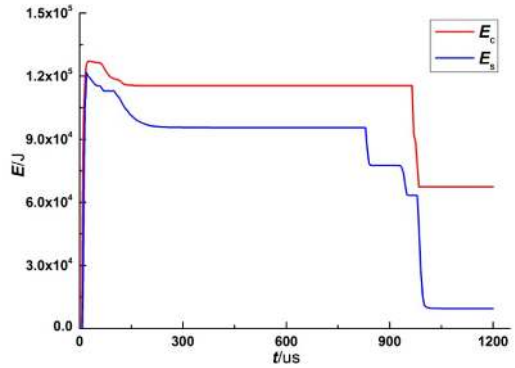


Figure 17: Energy changes of central and surrounding penetrator when the standoff is 1.7m.

The whole process of formation and penetration of MEFP is simulated by a 3D coupled hydrocode of LS-DYNA. Numerical results have successfully explained the distribution pattern of perforations on the target namely every surrounding liner is broken into three penetrators during the formation process of MEFP and a group of aimable penetrators consisted a central projectile surrounded by 18 penetrators is finally formed.

6 CONCLUSIONS

Experiments and three-dimensional numerical simulations have been performed to study the dispersion patterns and penetration properties of MEFP warhead with seven arc-cone liners. Once initiated, damage probability for defeating light armor can be significantly improved and the results provide important reference to the design and optimization of MEFP warhead in engineering. The major conclusions are as follows:

(1) A group of aimable penetrators consisting a central penetrator surrounded by 18 penetrators has been formed during the formation process of MEFP and moves in the direction of target. Maximum divergence angle of surrounding penetrators is 9.8° and the damage area can reach 0.37m^2 at 1.7m.

(2) A nonlinear surface fitting based on Gauss model has been established to describe dispersion patterns of MEFP according to perforations information on the witness target in the experiment. It can be expressed by:

$$Z = Z_0 + Ae^{-\frac{1}{2}(\frac{X-C_1}{W_1})^2-\frac{1}{2}(\frac{Y-C_2}{W_2})^2} \quad (Z \geq 0)$$

It provides a method to forecast damage area of MEFP if the distance between the MEFP warhead and target is measured, achieving good prediction about coverage pattern of MEFP.

(3) Terminal effects of MEFP remainder are investigated by the rear target in the experiment. After breaking down a 1.5 cm #45 steel target at different standoffs, the fragments distribution of MEFP becomes more dispersed and total energy of remainder gets relatively smaller as the standoff increases.

Acknowledgments

This research was supported by the State Key Laboratory of Explosion Science and Technology (KFJJ10-2M), the Advanced Research of PLA University of Science and Technology (201417) and Science Foundation of College of Filed Engineering (2015-7).

References

Blachel A. and Weimann K., (1999). Muti-EFP-Charge for Lightweight Armor Defeat. In. Proceedings of the 18th international symposium on ballistics, Sanantonio, Texas:15-19.

Chen G., Chen Z.F., Xu W.F., et al, (2007). Investigation on the J-C ductile fracture parameters of 45 steel. Explosive and Shock Waves 27:131-135,

D.Cardoso, F.Teixeira-Dias,(2016). Modelling the formation of explosively formed projectiles(EFP). International Journal of Impact Engineering 93:116-127.

David B., Richard F.,William Ng, et al, (2001). Dual mode warhead technology for future smart munitions. In. Proceedings of the 19th international symposium on ballistics,Interlaken,Switzerland: 679-684.

Hallquist J.O., (1997). LS-DYNA Theoretical Manual, Livermore Software Technology Corporation, Livermore, CA, USA.

Johnson C.R., Cook W.H.,(1983). A constitutive model and data for metals subjected to large strain, high strain rates and high temperature. In. Proceedings of the 7th International Symposium on Ballistics, Hague, Netherlands:541-548.

Johnson GR, Cook WH,(1985). Fracture characteristics of three metals subjected to various strains, strain rates, temperatures and pressures. Engineering Fracture Mechanics 21:31–48.

Johnson GR, Stryk RA,(2006). Some considerations for 3D EFP computations. International Journal of Impact Engineering 32:1621-1634.

Li W.B., Wang X.M., Li W.B.,(2010). The effect of annular multi-point initiation on the formation and penetration of an explosively formed penetrator. International Journal of Impact Engineering 37:414-424.

Li, Z.C., Zhu, Z.P. and Xue, J.F. ,1995, Steel Materials Handbook, China Materials Resource Publication,12.

M.A. Meyers, 1994, Dynamic Behavior of Materials, John Wiley and Sons Inc., New York.

Richard F., Matthew C., Henry H., Frank L., William Ng., (2010). Combined effects warhead evelopment, In. Proceedings of the 25th international symposium on ballistics, Beijing, China: 874-879.

Richard F., William Ng., Bernard R, et al, (2001). Multiple Explosively Formed Penetrator Warhead Technologies. In. Proceedings of the 19th international symposium on ballistics,Interlaken,Switzerland: 563-568.

Richard F., William Ng., Bernard R., et al, (2001). Multiple Explosively Formed Penetrator (MEFP) warhead technology development. In. Proceedings of the 19th international symposium on ballistics, Interlaken, Switzerland:563-568.

Richard F., William Ng., Steve Tang, et al, (2005). Multiple explosively formed penetrator (MEFP) warhead technologies for mine and improvised explosive device (IED) neutralization. In. Proceedings of the 22th international symposium on ballistics, Vancouver, BC Canada: 669-677.

S. Pappu, L.E.Murr,(2002). Hydrocode and microstructural analysis of explosively formed penetrators. Journal of material science 37:233-248.

Saroha R., Singh Y., Mahala V.K., (2010). Single point initiated multi-EFP warhead, In. Proceedings of the 25th international symposium on ballistics, Beijing, China: 1298-1302.

Wang H.F., Feng S.S.,(1998), Theoretical Initial Shock Properties of Porous Materials Under Explosion Loads, Journal of Beijing Institute of Technology, 18(5): 634-637.

Weickert C.A., (1990). Explosively Formed Projectile Clusters For Defeat of Soft Target. In. Proceedings of the 12th international symposium on ballistics, Sanantonio, Tesas:465-475.

Weickert CA, Gallagher PJ,(1993). Penetration of explosively formed projectiles. International Journal of Impact Engineering 14:809-818.

William Ng.,(2002). Long Standoff Demolition Warheads for Armor. Masonry and Concrete Targets, Mines, Demolition and Non-Lethal Conference 4 June.

Wu J., Liu J.B. and Du Y.X.,(2007). Experimental and numerical study on the flight and penetration properties of explosively-formed projectile. International Journal of Impact Engineering 34:1147-1162.

Ye X.S , 2003, Basis of dynamics explosion, Engineering Institute of Engineering Corps, PLA University of Science and Technology,238-245.

Yu C, Tong Y, Yan C,et al, (1999). Applied research of shaped charge technology. International Journal of Impact Engineering 23:981-988.

Zhao C. X., (2013). Technological researches on multiple explosive formed projectiles. PhD thesis, Nanjing: PLA University of Science and Technology.

Zhao C. X., Long Y., Sui Y. S., et al, (2012). Influence of initiation methods on formation of integral MEFP warhead parameter, Journal of PLA University of Science and Technology (Natural Science Edition) 13(5):559-564.

Zhao C. X., Qian F., Xu J. G., et al, (2016). Effect of liner configuration parameters on formation of integral MEFP, Chinese journal of energetic materials 24(5):485-490.

Zhao C. X., Qian F., Zhang H. Z., et al, (2015). Influence of liner material on formation of multiple explosively formed projectiles warhead parameters. Advanced Materials Research 1096:37-41.

Zhao C.X., Long Y., Ji C., et al, (2013). Numerical simulation and experimental research on integral multiple explosively formed projectile warhead. Acta Armamcntarii 34:1392-1397.